Yearly Variation of Acacia Plantation Forests Obtained by Polarimetric Analysis of ALOS PALSAR Data

Shoko Kobayashi, Yoshiharu Omura, Kazadi Sanga-Ngoie, Yoshio Yamaguchi, *Fellow, IEEE*, Ragil Widyorini, Motoko S. Fujita, Bambang Supriadi, and Shuichi Kawai

***Abstract*—Applications of remote sensing by microwaves have become widely adopted in forest management, but microwave backscattering mechanisms in plantations remain poorly understood. This study attempts to understand backscattering characteristics under different forest structural conditions in plantation forests of fast-growing acacia trees in Sumatra, Indonesia. A general four-component scattering power decomposition method was applied to ALOS PALSAR data collected from 2007 to 2010 to see the variations of acacia plantation. The yearly variation in decomposition powers was compared to forest inventory data with visual assessments of stand conditions. The results were highly consistent with the field-measured data. Based on the variation patterns of decomposition powers, we can identify the presence of understory and distinguish between damaged and well-grown stands. The PALSAR data analysis can also reveal partial damages within a forest compartment, even minor damage in younger forests. This in-depth study indicates that changes in forest stand composition and the growth and degradation of plantation forests can be monitored by transitions in the polarimetric parameters.**

***Index Terms*—Biomass, fast-growing trees, image decomposition, L-band, microwave imaging, plantation forests, polarimetry, radar remote sensing, synthetic aperture radar (SAR).**

I. Introduction

In RECENT years, industrial plantation forests have rapidly expanded throughout many parts of the world [1]. The rapid spread of plantations is regarded as an inevitable result of the increasing global demands for paper and oil products. Industrial plantations also pose a risk of environmental deterioration. Therefore, the sustainability of plantation forests must be ensured through continuous monitoring. Meanwhile, estimating the forest stand volume has also become important for commercial and forest management purposes.

Modern remote satellite sensing technology offers considerable benefit to earth environmental observations. In regions of persistent water vapor and clouds, which cannot be continuously monitored by optical sensors, microwave sensors are particularly advantageous because they operate well under all weather conditions. Radar imaging satellites are therefore considered the most suitable instruments for periodic forest monitoring in such regions. Among these advanced technologies is polarimetric synthetic aperture radar (PolSAR), which provides data with phase information. PolSAR has begun to be widely used for determining land cover and estimating above-ground forest biomass.

In PolSAR data analysis, land-use/land-cover or deforestation or forest regrowth is typically detected by a normalized radar cross section (σ^0) [2]–[5]. The σ^0 also detects stem volume and above-ground biomass [6]–[12]. Another emerging technique in forest analysis is polarimetric power decomposition. PolSAR target decomposition extracts surface features from polarimetry data [13]. Target decomposition is broadly divided into model-based [14] and eigenvalue-based [15] methods.

The model-based decomposition method developed by Freeman and Durden [14] resolves the three power components comprising surface, double-bounce, and volume (canopy) scatterings. This scheme was improved by adding a helix scattering term and by modifying the volume scattering model [16]. The four-component decomposition scheme was further improved through the introduction of a matrix rotation scheme that minimizes the volume scattering power and allows oriented urban areas to be distinguished as double-bounce scattering [17]. The four-component technique has also recently been further improved by Singh *et al.* [18] through the introduction of a unitary transformation to create new method known as general four-component decomposition (G4U). In the decomposition scheme, the helix term, together with other three (surface, double bounce, and volume) scattering powers, constitutes a complete model-based scattering mechanism that

Manuscript received August 29, 2014; revised September 18, 2015; accepted September 22, 2015. Date of publication October 26, 2015; date of current version January 18, 2016. This work was supported in part by a Grant-in-Aid for Young Scientists (B) from Japan Society for the Promotion of Science (JSPS KAKENHI Grant 25740006) and in part by a research grant for Mission Research on Sustainable Humanosphere from the Research Institute for Sustainable Humanosphere (RISH), Kyoto University.

S. Kobayashi is with the College of Agriculture, Tamagawa University, Machida 194-8610, Japan (e-mail: kshoko@agr.tamagawa.ac.jp).

Y. Omura and K. Sanga-Ngoie are with the Research Institute for Sustainable Humanosphere, Kyoto University, Kyoto 611-0011, Japan (e-mail: omura@rish.kyoto-u.ac.jp; sangank@rish.kyoto-u.ac.jp).

Y. Yamaguchi is with the Faculty of Engineering, Niigata University, Niigata 950-2181, Japan (e-mail: yamaguch@ie.niigata-u.ac.jp).

R. Widyorini is with the Faculty of Forestry, University of Gadjah Mada, Yogyakarta 55281, Indonesia (e-mail: ragil_w@hotmail.com).

M. S. Fujita is with the Center for Southeast Asian Studies, Kyoto University, Kyoto 606-8501, Japan (e-mail: fujita@cseas.kyoto-u.ac.jp).

B. Supriadi is with the Research and Development, PT. Musi Hutan Persada, Sumatera Selatan 31172, Indonesia (e-mail: Bambang-S@jpn.mhp.co.id).

S. Kawai is with the Graduate School of Advanced Leadership Studies, Kyoto University, Kyoto 606-8315, Japan (e-mail: kawai.shiyuuichi.3m@kyoto-u.ac.jp).

Color versions of one or more of the figures in this paper are available online at http://ieeexplore.ieee.org.

Digital Object Identifier 10.1109/JSTARS.2015.2487503

employs 100% of polarimetric information. No other model-based decomposition method accomplishes this 100% use of polarimetric information.

A few studies have attempted to retrieve forest structural parameters, such as tree diameter, height, and trunk volume, from the scattering power decomposition images of PolSAR data. Garestier *et al.* [19] implemented an eigenvector decomposition scheme. They reported a linear correlation between anisotropy derived from P-band data and the height of pine trees. Gonçalves *et al.* [20] reported that the volume scattering and several other backscattering coefficients are useful for extracting tropical forest information from L-band data. Notably, the targets in both of these studies [19], [20] were thick-stemmed trees, and the studied tropical forests had a dense canopy [20]. Fast-growing trees with thin trunks and low canopy densities have been little investigated. Among the few published studies on the subject, the biomass of fast-growing trees in commercial eucalyptus plantations has been estimated from the backscattering coefficients derived from JERS-1 single-polarization synthetic aperture radar (SAR) images [21] and interferometry SAR [22].

The accuracy of estimated forest stand attributes is well known to be site-dependent [23], [24] and affected by forest structures [25], [26], the shapes and dimensions of leaves and stems [27], and ground conditions. The backscattering characteristics of acacia trees, however, remain poorly understood.

In our previous analysis [28] using advanced land observing satellite (ALOS) phased array-type L-band synthetic aperture rader (PALSAR), we find that the σ^0 is weakly correlated with the forest structural parameters (coefficient of determination: $R^2 = 0.13$ for copolarizations and $R^2 = 0.29$ for cross-polarization with trunk volume). In addition, using optical advanced visible and near infrared radiometer type 2 (AVNIR-2), the normalized difference vegetation index (NDVI) of trees older than 2 years decreases with age (correlation coefficient: $r = -0.88$; $R^2 = 0.78$). We reported linear correlations between the decomposition powers derived by the four-component decomposition method [17] and forest metrics [29]. However, backscattering mechanisms were not considered in these analyses.

In this study, we observed the changes in plantation forests of fast-growing acacia trees by polarimetric analysis of Quad-pol SAR data collected from 2007 to 2010. We compared the yearly variations between scattering powers and forest inventory data with visual assessment of stand conditions. From the results, we elucidated how the fundamental characteristics of radar backscattering vary with forest structures and conditions.

II. Study Area

The study area is an industrial plantation forest located in the southeastern part of Sumatra Island, Indonesia (Fig. 1). The plantation mostly comprised a single-layered forest of *Acacia mangium*, a fast-growing tree that was normally harvested in this region approximately 6 years after planting the seedlings. Under the approval of the Indonesian Government, tree planting began in 1990 on deforested and unproductive sites initially overgrown with *alang-alang* (*Imperata cylindrica*) [30].

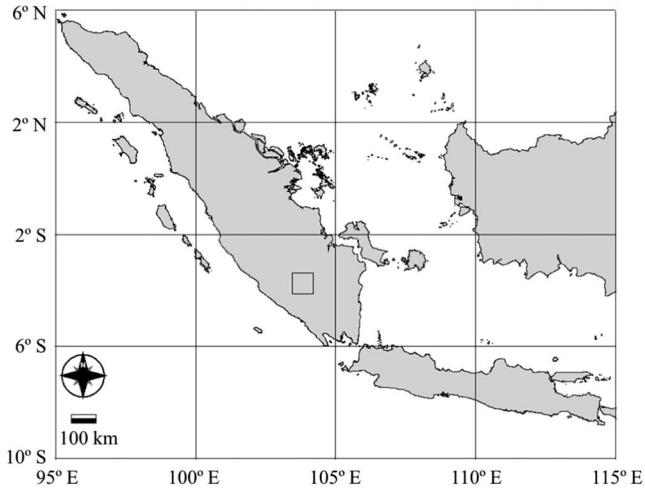

Fig. 1. Location of the study area in Sumatra, Indonesia (small black square).

The whole area managed by the planting company is divided into several units (called unit). Then, the unit is divided into practical management units called a forest compartment in which planting and harvesting are more-or-less simultaneously implemented. Our study targeted one of these units (Unit V) situated between latitudes $3°36'48''$S and $3°58'54''$S and longitudes $103°50'42''$E and $103°58'23''$E. The area covers 282.9 km^2, spanning about 15 km from east to west and 40 km from north to south. In 2007, Unit V included 3068 forest compartments covering 134.9 km^2. In 2009, 3764 compartments covered 136.7 km^2; in 2010, coverage had expanded to 140.4 km^2 with 4019 compartments. Less than 50% of the total area was actually planted, indicating that much of the area had been left to natural regeneration.

The altitude of the site ranges from 41 to 253 m (average 111.5 m) above sea level and is sloped between $0°$ and $14.9°$ (average $3.4°$). The climate is tropical with a dry season prevailing between June and September, and a rainy season prevailing between October and May. Two rainfall peaks occur in December–January and March–April. The mean annual rainfall varies from 2000 to 3000 mm.

III. Data Sets

A. Field Measurement Data and Compartment Boundaries

Forest inventory plots were randomly allocated. Within the rhomb-shaped perimeter of each plot (diagonal $= 31.6$ m), individual trees were placed 3 m apart in a triangular pattern, such that each plot contained 60 standing trees. From the acquired satellite data (see Section III-B), the number of plots was 32, 49, and 47 in 2007, 2009, and 2010, respectively (Fig. 2). All of the forest inventory plots had been originally planted with acacia trees. Note that the location of the forest inventory varied, as the forest compartment boundaries were rearranged.

Yearly observations of each plot on a rotating basis carried out in order to obtain forest structural metrics and visual assessment data. The forest structural metrics included 1) tree diameter at breast height (DBH) in centimeters; 2) standing

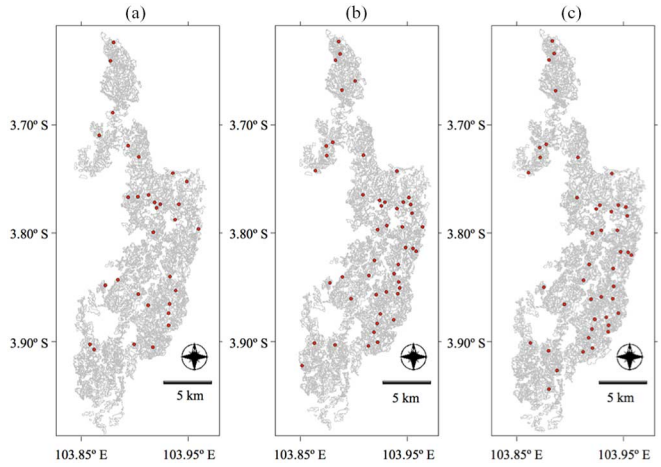

Fig. 2. Background shown by gray-colored line presents forest compartment boundary in Unit V. Red circles mark location of the forest inventory plots in which the field measurements were conducted in (a) 2007; (b) 2009; and (c) 2010.

tree height (H) in meters; and 3) trees per hectare (N). The DBH and H were measured by a diameter tape and clinometer, respectively, and averaged over each plot. Another structural metric, the tree form factor (F) of the *Acacia mangium* stems, was measured as 0.48 from felled tree samples [31]. The visual assessment data are collected by the experienced local staff.

Herein, we emphasize that tree age refers to the number of years elapsed since the planting date. The seedlings are typically 3 months old when planted. Forest compartment boundaries (Fig. 2) were delineated by a global positioning system (GPS).

B. Microwave Satellite Remote Sensing Data

We used ALOS-PALSAR SAR full-polarimetry data with HH/HV/VV/VH, acquired on May 20 2007, April 09 2009, and April 12 2010 with an off-nadir angle of 21.5° in ascending orbit. The PALSAR sensors operated in the L-band and were spatially resolved to 30 m in the range direction and 5 m in the azimuthal direction in the polarimetry mode. Here, we emphasize that data were taken only in 2007, 2009, and 2010; no data were collected in 2008. The data sets are provided by the Japan Aerospace Exploration Agency (JAXA) at processing Level 1.1.

IV. Methods

A. Polarimetric Data Analysis

We applied the G4U [18], which confers several advantages over previous scattering power decomposition methods. G4U accounts for all polarimetric parameters contained in the coherency matrix, which implies that G4U uses 100% polarimetric information in the decomposition and computes positive decomposition powers. Four-component scattering decomposition methods were originally developed for urban settings by adding a helix scattering power that is equal to the circular polarization power [16]. However, they are also applicable to more general settings, as they can theoretically decompose any polarimetric data. In addition, the helix scattering power can be caused by spaced dipole structures (such as branches in forests), which is dependent on frequency.

1) Speckle Noise Reduction and Ensemble Averaging: Each element of the scattering matrix $[S]$ contains complex numbers denoted by S_{HH}, S_{HV}, S_{VV}, and S_{VH}. In the case of reciprocity, where $S_{\mathrm{VH}} = S_{\mathrm{HV}}$, a 3×3 complex coherency matrix $[T]$ relating to the second-order statistics of the scattering matrix elements is given in terms of the Pauli vector k_{p} by

$$[T] = k_p k_p^{\dagger} = \begin{bmatrix} T_{11} & T_{12} & T_{13} \\ T_{21} & T_{22} & T_{23} \\ T_{31} & T_{32} & T_{33} \end{bmatrix} \tag{1}$$

$$k_p = \frac{1}{\sqrt{2}} \begin{bmatrix} S_{HH} + S_{VV} \\ S_{HH} - S_{VV} \\ 2S_{HV} \end{bmatrix} \tag{2}$$

where † denotes complex conjunction and transposition [32]. To determine the ensemble average of the coherency matrix $\langle [T] \rangle$ (3), a moving average filter with window size 2×12 (2 pixel in the range direction; 12 pixels in the azimuth direction) was then applied to each element

$$\langle [T] \rangle = \langle k_p k_p^{\dagger} \rangle \tag{3}$$

where $\langle\ \rangle$ denotes the ensemble averaging in the data processing. The window size corresponds to 60 m $\times$ 60 m on the ground. In addition, considering both inventory plot size (see Section III) and complicated shapes of forest compartments (Fig. 2), we selected the 2×12 window size to ensure high accuracy.

2) General Four-Component Scattering Power Decomposition With Unitary Transformation: To account for all polarimetric parameters contained in the coherency matrix, the algorithm performs two unitary transformations. The rotated matrix $\langle [T(\varphi)] \rangle$ containing the observed SAR data is decomposed into four distinctive scattering powers: surface scattering (P_{s}), canopy (volume) scattering (P_{c}), double-bounce scattering (P_{d}), and helix scattering (P_{h})

$$\begin{aligned} \langle [T(\varphi)] \rangle = {} & f_s \langle [T(\varphi)] \rangle_s + f_c \langle [T(\varphi)] \rangle_c + f_d \langle [T(\varphi)] \rangle_d \\ & + f_h \langle [T(\varphi)] \rangle_h \end{aligned} \tag{4}$$

where f_{s}, f_{c}, f_{d}, and f_{h} are the expansion coefficients, and $\langle [T(\varphi)] \rangle_{\mathrm{s}}$, $\langle [T(\varphi)] \rangle_{\mathrm{c}}$, $\langle [T(\varphi)] \rangle_{\mathrm{d}}$, and $\langle [T(\varphi)] \rangle_{\mathrm{h}}$ are their corresponding scattering models. The decomposition powers were calculated from the traces of each term in (4): $f_{\mathrm{s}} \langle [T(\varphi)] \rangle_{\mathrm{s}}$, $f_{\mathrm{c}} \langle [T(\varphi)] \rangle_{\mathrm{c}}$, $f_{\mathrm{d}} \langle [T(\varphi)] \rangle_{\mathrm{d}}$, and $f_{\mathrm{h}} \langle [T(\varphi)] \rangle_{\mathrm{h}}$.

Although the term "volume scattering" is usually subscripted by "v," we here adopt "canopy scattering," subscripted by "c," to avoid confusion. Consequently, we replace the subscript "c," which is usually assigned to helix scattering, by "h."

Each decomposition power is divided by the total power (TP): P_{s}/TP, P_{c}/TP, P_{d}/TP, and P_{h}/TP. These normalized powers (P/TPs) are more highly correlated with the forest structural metrics than the nonnormalized powers [29]. Using the P/TP, we can quantify the interrelations among the backscattering from the targets, and thereby better understand the backscattering mechanisms.

B. Preprocessing of Data Sets

1) Geometric Correction of SAR Data: The PALSAR data had been calibrated into Level 1.1 data by JAXA. Therefore, we first corrected the incidence angle of the radar beam and registered it to the Universal Transverse Mercator (UTM) coordinate system. To this end, we applied slant-to-ground range corrections to the SAR images. To obtain square pixels accommodating the buffer width (see Section IV-B3), the pixel spacing was set to the ground resolution of 15 m in both cross-track and along-track directions. The grid system definition was followed by an inverse distance weighted (IDW) interpolation with unity weighting factor. Given the flat topography of the forest compartment areas (average slope $= 3.4°$), we assumed that the relief exerts negligible influence, and therefore disregarded the local topographic effects.

2) Forest Structural Metrics: The field measurement data (DBH, H, and N) were linearly interpolated between their values to obtain the correct values at the satellite acquisition dates. This procedure was required, because the forest inventory data were collected throughout the year: the forest inventory plots were ground-surveyed at different times that also differed from the acquisition dates of the satellite imagery. Forest measurements were constantly conducted once a year. Therefore, the results between linear and high-order interpolations make slight differences. In addition, simple linear interpolation would be suitable, because higher order schemes may cause a significant error when there is observation error.

From the obtained forest metrics, the trunk volume per hectare (V) in m^3/ha was calculated with the formula

$$\mathrm{V} = \pi \times (\mathrm{DBH} \times 10^{-2}/2)^2 \times \mathrm{H} \times \mathrm{F} \times \mathrm{N}. \tag{5}$$

3) Polygon Vector Layer of Forest Compartment Boundary: Vector data of the forest compartments were coregistered according to the georeferenced satellite imagery by ground control points (GCPs) with a first-order polynomial transformation. The total root-mean-squared error (RMSE) was 8.27 m. In order to reduce mixed-pixel effects at the boundaries and minimize geographic errors, the forest compartment areas were reshaped by a buffer operation. Buffering was used for discarding the pixels on the boundaries and within the designated buffer zone. Based on the RMSE (8.27 m) and the PALSAR resolution (30 m), the spatial buffer width was set to 15 m from the boundary line. In addition, we considered forest compartments covering less than 0.01 km^2 were unsuitably small, and excluded them from the analysis.

C. General Correlation Analysis

We conducted a general correlation analysis to obtain the overall relationships between the forest metrics and P/TPs. In each year (2007, 2009, and 2010), the linear dependences between the base 10 logarithm of each forest metric ($\log_{10}$DBH, $\log_{10}$H, and $\log_{10}$V) and the normalized decomposition powers (P_s/TP, P_c/TP, P_d/TP, and P_h/TP) were evaluated. The logarithmically converted forest metrics are expected to yield linear relationships because acacia trees grow rapidly within the first 2–3 years; thereafter, their growth slows with age [28]. The forest stand metrics were similarly transformed to logarithmic form for investigating their relationships with microwave backscatter [21], [22].

The analysis was conducted on forest compartments with the forest inventory plot; 27 compartments covering 1.74 km^2 in 2007, 43 compartments covering 3.06 km^2 in 2009, and 42 compartments covering 2.70 km^2 in 2010. The satellite data were processed by computing the means of the P/TPs over the various forest compartments. Each compartment contained a single inventory plot. Forest management practices essentially ensure that each forest compartment is a uniform entity. Although this assumption does not always hold, the analysis at the forest compartment scale is well compatible with the practical forest management and was applied throughout this study. The satellite information over a forest compartment is frequently averaged in correlation analyses involving forest metrics [19], [20], [26], [33].

D. Transition of Decomposition Powers From 2007 to 2010

To investigate the backscattering characteristics further, we tracked the changes in the P/TP values and compared them to the corresponding forest metrics. The transition analysis from 2007 to 2010 (excluding 2008) was conducted over the forest inventory plots and in forest compartments with shared boundaries over the study period that were not altered between rotations as part of forest management practices. We selected nine inventory plots, and numbered them in ascending order of planting date as Plots 1–9.

V. Results

A. Composite of Scattering Power Decomposition Images

Fig. 3 shows RGB composite images (RGB $= P_\mathrm{d}/TP$, P_c/TP, P_s/TP) compiled for each year. Regions dominated by blue indicate areas of newly planted seedlings or between harvesting and planting periods, where the grounds are exposed and the dominant component is P_s/TP. Green regions show areas of strong P_c/TP, which are dominated by the vegetation cover. Reddish pixels indicate a higher ratio of P_d/TP and are rarely seen in the images. Between 2007 and 2010, some blue-dominated areas become green and vice versa.

B. General Correlation Between In Situ Forest Measurement Data and Remotely Sensed SAR Data

Scatter plots and least-squares regression lines between each of $\log_{10}$DBH, $\log_{10}$H, and $\log_{10}$V on the x-axis and each of P_s/TP, P_c/TP, P_d/TP, and P_h/TP on the y-axis were plotted for each year of the study. The $\log_{10}$V plots are shown in Fig. 4 (the $\log_{10}$DBH and $\log_{10}$H plots are not shown). Table I presents the Pearson's correlation coefficients (r) and p-values. The correlation trends among the forest metrics and also among each of the scattering powers are very similar.

The forest metrics are negatively correlated with P_s/TP ($r = -0.60$ to -0.78), but are positively correlated with

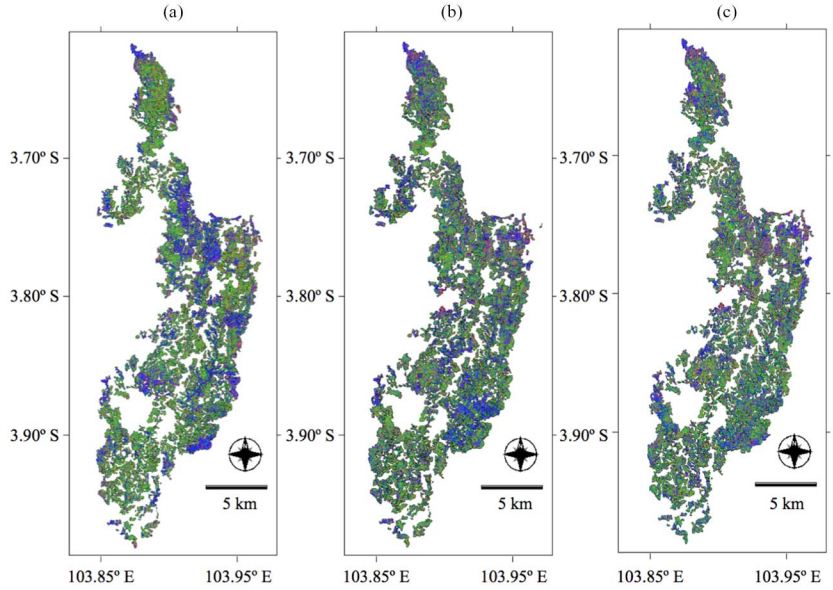

Fig. 3. Composite images of scattering power decomposition images (RGB = double-bounce/canopy/surface scatterings) for (a) 2007; (b) 2009; and (c) 2010.

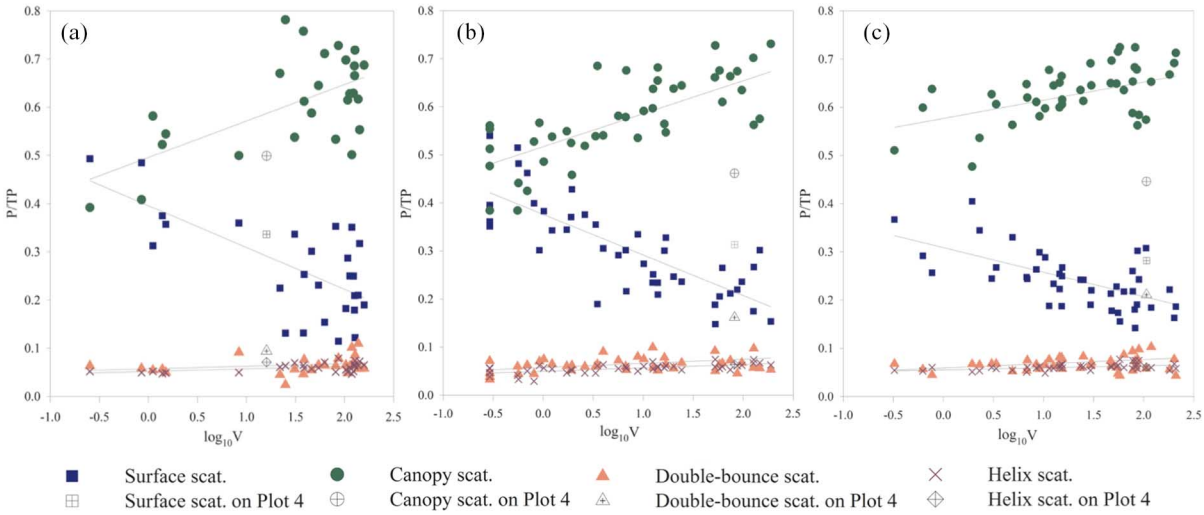

Fig. 4. Scatter plots and regression lines between the base 10 logarithms of the forest stand volume ($\log_{10}$V) on the x-axis and the normalized decomposition powers (P/TP) on the y-axis for (a) 2007; (b) 2009; and (c) 2010. Blue, green, and red represent the normalized surface scattering: $P_{\rm s}/TP$, canopy scattering: $P_{\rm c}/TP$, and double-bounce scattering: $P_{\rm d}/TP$, respectively, and purple cross mark represents the helix scattering: $P_{\rm h}/TP$. The decomposition powers on the Plot 4 are shown by plus marks in square symbol for $P_{\rm s}/TP$, in circle for $P_{\rm c}/TP$, in triangle for $P_{\rm d}/TP$, and in diamond for $P_{\rm h}/TP$.

$P_{\rm c}/TP$ ($r = 0.40$ to 0.69), $P_{\rm d}/TP$ ($r = 0.21$ to 0.45), and $P_{\rm h}/TP$ ($r = 0.46$ to 0.70). The correlations are higher in 2009 than in 2007 and 2010, and lower in $P_{\rm d}/TP$ than in the other scatterings.

It should be noted that the P/TPs on Plot 4, while measuring up to the trunk volume in 2007 [Fig. 4(a)], are clearly recognized as outliers in 2009 and 2010 [Fig. 4(b) and (c)], in which the $P_{\rm c}/TP$ and $P_{\rm h}/TP$ were much lower and higher than expected, respectively. The values on Plot 4, labeled by plus symbols in Fig. 4, were excluded from the correlation calculation.

C. Yearly Variations in Decomposition Powers

Yearly variations of P/TPs in the forest compartments holding Plots 1–9 are shown in Fig. 5. Here we summarize the characteristics of each stand. Plots 1–9 are placed into categories (1)–(6), depending on their planting dates and tree growth rates. Fig. 5 contains descriptions of the visual assessment results of each stand condition. These will be discussed in comparison with variation of decomposition powers in the next section.

1) Plot 1 [Fig. 5(a)]: Plot 1 uniquely holds both harvesting and planting records between 2007 and 2010. These manifest as clear dips in the graphs of the forest metrics. The first planting was performed in December 2003, followed by harvesting and the second planting in February 2009. A few months after the second planting, the satellite collected data. The harvesting practice induced a remarkable change in $P_{\rm d}/TP$ and $P_{\rm h}/TP$, while the other P/TPs were less affected. The composite image in Plot 1 changes from green to bluish between 2007 and 2009, returning to

TABLE I
CORRELATION COEFFICIENTS (R) AND THE P-VALUES BETWEEN FOREST METRICS ($\log_{10}$DBH, $\log_{10}$H, AND $\log_{10}$H) AND THE NORMALIZED DECOMPOSITION POWERS (P_s/TP, P_c/TP, P_d/TP, AND P_h/TP)

		In situ data (Field-measured forest parameters)								
		2007			2009			2010		
		DBH	Height	Volume	DBH	Height	Volume	DBH	Height	Volume
Remotely sensed data	*Ps/TP*	−0.694 (< 0.001)	−0.685 (< 0.001)	−0.687 (< 0.001)	−0.777 (< 0.001)	−0.775 (< 0.001)	−0.782 (< 0.001)	−0.603 (< 0.001)	−0.608 (< 0.001)	−0.612 (< 0.001)
	Pc/TP	0.626 (< 0.001)	0.620 (< 0.001)	0.614 (< 0.001)	0.687 (< 0.001)	0.660 (< 0.001)	0.685 (< 0.001)	0.395 (0.009)	0.414 (0.006)	0.426 (0.004)
	Pd/TP	0.231 (0.237)	0.209 (0.285)	0.249 (0.202)	0.373 (0.013)	0.446 (0.002)	0.393 (0.008)	0.300 (0.053)	0.271 (0.079)	0.248 (0.109)
	Ph/TP	0.461 (0.014)	0.476 (0.011)	0.479 (0.010)	0.656 (< 0.001)	0.704 (< 0.001)	0.668 (< 0.001)	0.482 (0.001)	0.461 (0.002)	0.465 (0.002)

green in 2010. Because of its relatively low proportion, P_d/TP does not appear on the composite image.

2) Plots 2 and 5 [Fig. 5(b) and (e)]: Planted in 2004, these trees were about 2.5 years old in 2007. A high growth rate was found; the trunk volume was approximately 200 m^3/ha in 2010, when the trees were 5 years old. In Plot 2, the P_c/TP continuously increased while the other three P/TPs decreased. Meanwhile, in Plot 5, the P_c/TP notably decreased between 2007 and 2009 and increased in 2010, the other three P/TPs increased between 2007 and 2009, and declined in 2010. The pixels in the composite image gradually become greener from 2007 to 2010.
3) Plot 3 [Fig. 5(c)]: Planted in 2004, these trees grew slowly, at less than half the growth rate of trees in Plots 2 and 5. The decrease in P_c/TP in 2010 was accompanied by a significant increase in P_d/TP and a slight increase in P_s/TP and P_h/TP.
4) Plot 4 [Fig. 5(d)]: Plot 4 shows distinctive changes, manifesting a significant increase in P_d/TP and continuous decline in P_s/TP, P_c/TP, and P_h/TP. The composite images partially redden in 2009 and 2010.
5) Plots 6 and 8 [Fig. 5(f) and (h)]: Planting was carried out in late 2006 and early 2007. Trees were 0.5 years old in 2007 and showed a good growth rate during the growing phase. Whereas the P_s/TP notably decreased between 2007 and 2009 and increased in 2010, the P_c/TP significantly increased between 2007 and 2009, and largely declined in 2010. Meanwhile, the P_d/TP gradually increased throughout the 3-year study period. The P_h/TP changed in the same way with P_c/TP in Plot 6, while it continued to increase slightly in Plot 8. The composite image changes from blue to green between 2007 and 2010, but some regions reverse to blue in the 2010 image.
6) Plots 7 and 9 [Fig. 5(g) and (i)]: Planting dates in early 2007 almost coincided with those of Plots 6 and 8, but these trees grew at a faster rate. The P_c/TP significantly increased between 2007 and 2009; thereafter, it just slightly decreased. The P_s/TP continuously decreased, apart from a slight increase in Plot 7 between 2009 and 2010. The P_d/TP showed a gradual increase, except for a slight decrease in Plot 7 between 2009 and 2010. The P_h/TP continued to increase slightly throughout 3 years. Overall, the composite image changes from blue to green, remaining blue in some regions.

VI. DISCUSSION

A. General Correlation Between Decomposition Powers and Forest Structural Metrics

Gonçalves *et al.* [20] applied the Freeman and Durden decomposition approach to airborne L-band SAR data. They reported that all scattering contributions to the total power positively correlate with the trunk volume of the tropical forests.

In the present study on multiyear polarimetric data, relative surface scattering (P_s/TP) was significantly negatively correlated with the forest metrics, whereas relative canopy, double-bounce, and helix scatterings (P_c/TP, P_d/TP, and P_h/TP) were positively correlated with these metrics (Fig. 4). These relationships can be understood as follows: as the forests grow 1) less bare ground is exposed, which reduces the surface scattering; 2) expanding vegetation increases the canopy scattering, which results from collections of randomly oriented leaf scatterers; 3) the growth of tree trunk and height increases the double-bounce scattering, which is generated from perpendicular ground–trunk intersections; and 4) the helix scattering, which is generated from spaced dipole structures such as branches, increases. Overall, these correlations are consistent with tree growth.

Note that decreased correlation in the double-bounce scattering is caused by the following facts: 1) young forest compartments showed linear positive correlations with forest growth; meanwhile 2) healthy mature stands with larger trunk volumes showed lower P_d/TP; and 3) damaged stands with medium trunk volumes exhibited higher P_d/TP. The details of the backscattering behaviors of the double-bounce scattering and damage to the trees are described in Section VI-B2.

The correlations were higher in 2009 than in 2007 and 2010 (Table I). We inferred that the interannual correlation differences most likely arise from changes in moisture contents of the ground and forest canopy. Moisture increases the backscattering from targets. In addition, the short-term and diurnal water statuses are altered by transpiration [13], [34]. Therefore, in future work, we should investigate the dielectric constant of the vegetation.

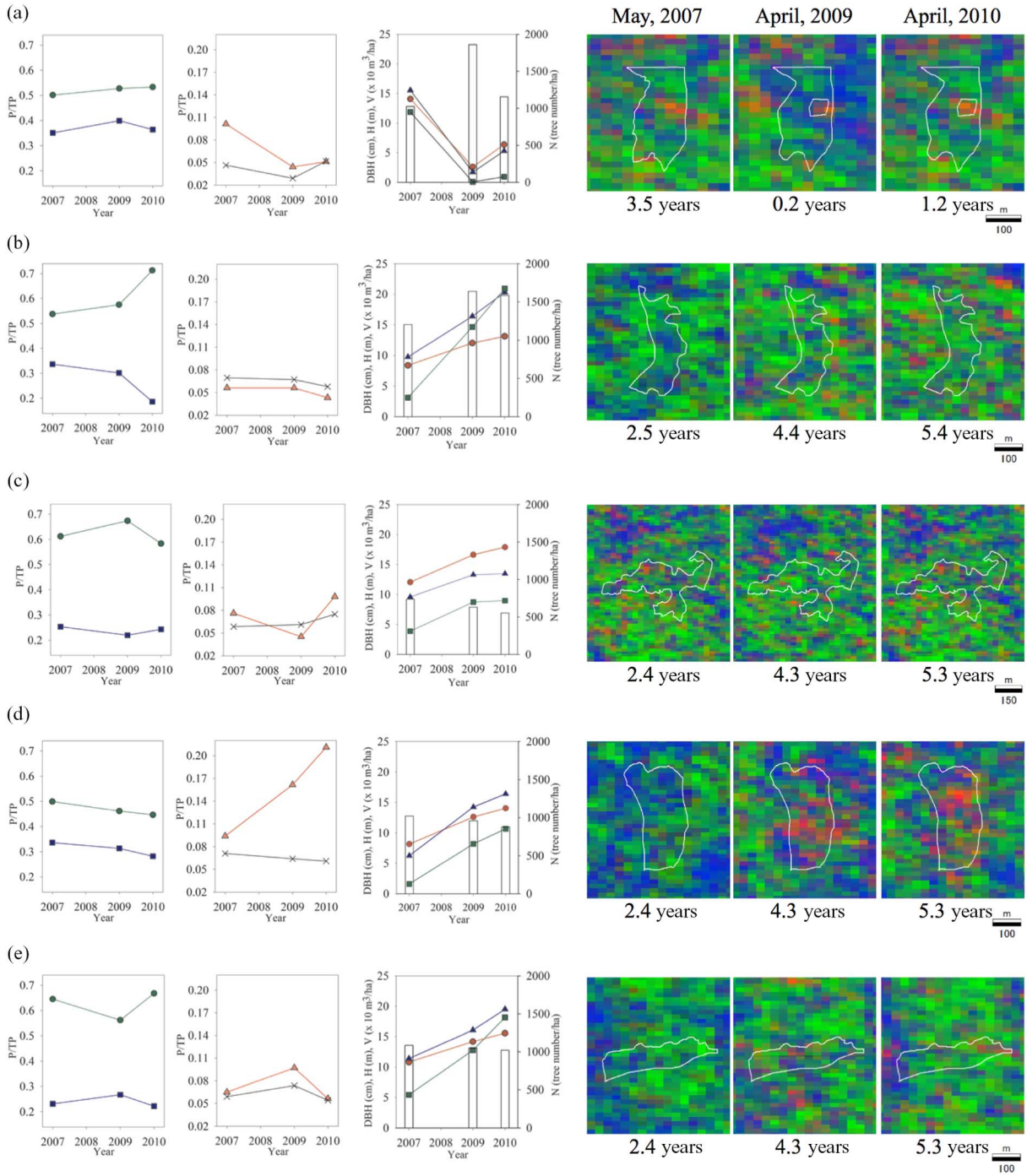

Fig. 5. (a)–(i) Plots 1–9, respectively. (Leftmost columns) Line graphs of the surface and canopy scattering powers normalized by total power in blue and green, respectively. (Second columns from the left) Line graphs of the double-bounce and helix scattering powers normalized by total power in red and gray lines, respectively. (Third columns from the left). The forest structural metrics shown by red lines for DBH, blue lines for height, and green lines for trunk volume. Bar graphs show tree number per hectare. [Right three columns] Composite images (RGB = double-bounce, canopy, and surface scattering) with forest compartment boundaries. Tree age in year on the date of satellite overpass is, respectively, shown at the bottom of the image. (a) Plot 1, planted in December 2003 and on February 2009; likely damaged but trees still survived before harvested in January 2009. (b) Plot 2, planted in November 2004; undamaged till harvested. (c) Plot 3, planted in December 2004; very damaged, field measurements were fluctuated. (d) Plot 4, planted in December 2004; significantly damaged, but trunks were regularly distributed. (e) Plot 5, planted in December 2004; undamaged till harvested. (f) Plot 6, planted in December 2006; slightly damaged in December 2009, damaged in January 2009. (g) Plot 7, planted in January 2007; undamaged in January 2010, small damaged in July 2010. (h) Plot 8, planted in January 2007; damaged between January 2008 and July 2010. (i) Plot 9, planted in May 2007; undamaged.

B. Understanding of Forest Structural Conditions via Decomposition Powers

This section suggests reasons for backscattering behaviors under different forest structural conditions. Herein, we observed the yearly variations in the polarimetric decomposition powers against forest inventory data, which were obtained by both forest measurements and visual assessment of the stand conditions (see Fig. 5).

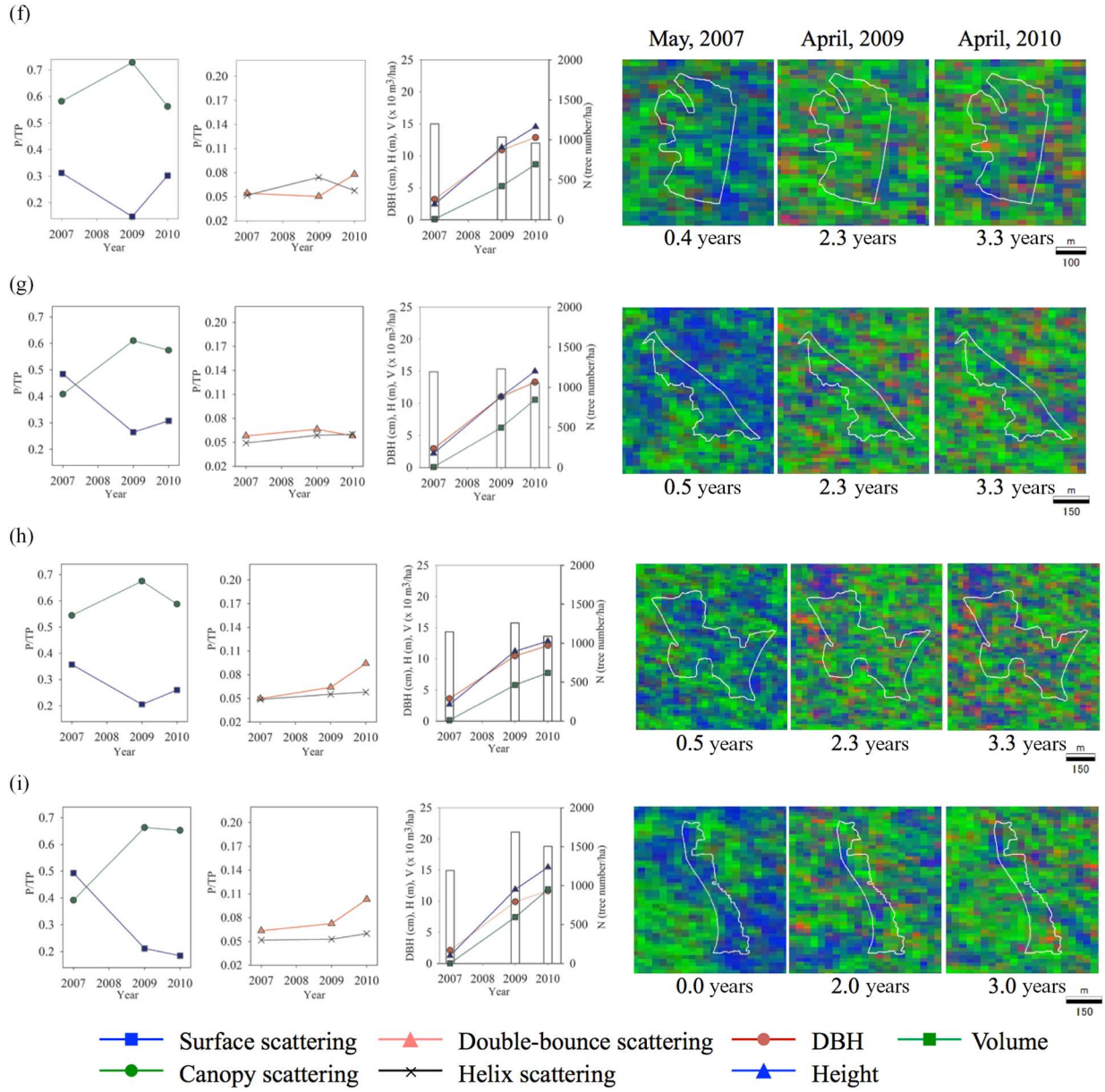

Fig. 5. (*Continued.*)

1) Understory Growth Following the Growing Phase: The canopy scattering from this plantation is very likely influenced by both forest canopy and understory vegetation. The canopy cover reduces after the 0–2 year growing phase [28], rendering the near-ground environment more favorable for understory growth. The understory growth increases the canopy scattering even while the forest leaves gradually decrease. The above discussion is supported by the following results.

1) The P_c/TP was strongly positively correlated with tree growth (Table I), which shows continuous increase of vegetation cover.
2) The optical NDVI gradually decreases after the growing phase until the harvesting time [28]. Since the wavelengths sensed by optical sensors are too short to penetrate the forest canopy layer [36], decreased NDVI indicates fewer tree leaves. Indeed, a thinning forest canopy has been actually observed in the mature stands.
3) Plots 2 and 5 were visually assessed as undamaged until harvested. The P_c/TP significantly increased between 2009 and 2010, when the trees had matured.

The obtained results indicate the appearance of vegetation other than acacia trees during the mature phase. It is also unlikely that rapid expansion of acacia tree canopy would take place after the growing phase.

The field observation in this plantation by Fujita *et al.* [35] strongly supports our interpretation of the images. They mention that the appearance of understory vegetation had already been observed in 4-years-old acacia forests with average understory covers of 29% and 60% at 1–10 m and 0–1 m in height, respectively. Moreover, one-year-old planted acacia was the dominant species in younger compartments with an average understory cover of 3% at 0–1 m in height.

2) Decrease of Double-Bounce Scattering by Vegetation Cover: Since double-bounce scattering theoretically reflects

trunk volume [13], it should linearly increase with tree growth. However, the correlations between P_{d}/TP and forest metrics were low (Table I), probably because the forest canopy and understory vegetation interfered with the proportional relation between them. This phenomenon explains the reduced P_{d}/TP that characterized mature (5–6 years old) healthy forest compartments. These conclusions are based on the following results.

1) Plots 2 and 5, which contained understory vegetation (see Section VI-B1), exhibited strong P_{c}/TP but weakened P_{d}/TP in 2010 [Fig. 5(b) and (e)]. Theoretically, these plots with the largest trunk volume should display the highest double-bounce scattering power.
2) Visual inspection revealed that the canopy leaves of Plot 4 were severely damaged, and tree trunks were regularly distributed. The P_{c}/TP and P_{d}/TP were decreased and increased, respectively [Fig. 5(d)], despite the medium trunk volume.
3) Damaged stands were found in Plot 3 (although the time of damage onset could not be determined). In 2010, the P_{c}/TP in this plot suddenly decreased, accompanied by a sharp increase in the P_{d}/TP.

Note that a fungus invading trees and a monkey pealing the bark generally caused tree damages, such as leaf dying and forest dieback, in this plantation.

The phenomenon is supported by Ryerson *et al.* [34], who reported that vegetation layers strongly influence the trunk-ground double bounce. Therefore, in determining the forest stand attributes, the effect of the understory environment cannot be ignored, and the trunk volume should not be estimated solely from the double-bounce scattering power.

Tree density has a certain level of effect on double-bounce scattering power. However, the results of this study did not show a definite correlation between double-bounce scattering mechanism and tree density [Fig. 5(a)–(i)], suggesting that complexity in the forest layer structure also affect double-bounce scattering, beside trunk volume and tree density.

3) Physical and Ecological Significance of Applying Four-Component Decomposition in Forested Areas: First, four-component decomposition has an advantage in terms of full exploitation of polarimetric information. Helix scattering power itself is not significant in comparison with other powers. However, the important factor in this decomposition is 100% polarimetric information usage. With helix scattering, the decomposition result consequently becomes more accurate than that of any other model-based scattering decompositions.

Second, the helix scattering is also derived from dipole structures such as branches in forests, although the scattering effectively distinguishes artificial structures [16]. Here, we can logically hypothesize that growth of understory vegetation in acacia plantation could be distinguished from canopy growth of the tree itself, by checking helix scattering together with canopy scattering. Consequently, helix scattering term should be considered as an important component, especially in sparse forests. This idea is supported by the following results.

1) The P_{c}/TP was significantly increased between 2007 and 2009 on Plots 6–9, containing younger trees in the growth phase (0–2 years old) [Fig. 5(f)–(i)]. At the same time, it was accompanied by increase in the P_{h}/TP. The increase in both canopy and helix scatterings indicates growth of the tree itself.
2) Conversely, a sharp increase in P_{c}/TP between 2009 and 2010 took place with a decrease of P_{h}/TP in Plots 2 and 5 [Fig. 5(b) and (e)], which had undamaged trees with understory vegetation (as mentioned in Section VI-B1). In the case where it is accompanied by a decrease of the helix scattering, an increasing canopy scattering trend does not indicate canopy growth but understory growth (as mentioned in Section VI-B1). That is because the helix scattering component is less affected by the understory than by branches in the canopy.

As a consequence, the inverse relationship, in which an increase in the canopy scattering and a decrease in the helix scattering take place simultaneously, arises from the existence of understory vegetation. The present data support this hypothesis, though further confirmation is needed.

C. Monitoring of Plantation

The yearly variation analysis suggests that, by decomposition powers from polarimetric L-band SAR data, we can monitor the vegetative growth and changes in forests. The obtained variations were consistent with forest inventory data. The main findings are discussed as follows.

1) In the visual assessment, Plots 2, 5, and 9 were undamaged. In healthy mature stands, the P_{c}/TP is significantly increased before harvest time or in mature period, while the P_{d}/TP and P_{s}/TP are decreased by the remaining tree canopy and generated understory vegetation. In healthy younger stands, plots exhibit few-decreased P_{c}/TP because of intact closed canopies.
2) The leaves in Plots 3 and 4 were severely damaged. This damage is reflected by the decreased P_{c}/TP and significantly enhanced P_{d}/TP.
3) The visual assessment data confirmed leaf damage in Plots 6 and 8 in 2010. The P_{c}/TP was significantly reduced in the stands between 2009 and 2010. The increased surface and double-bounce scatterings derived from the thinning forest canopy. The ALOS PALSAR data detect the damage and incidence, which occurred only within 1 year.
4) Among the young tree compartments, Plot 7 already showed a decrease of the P_{d}/TP between 2009 and 2010. That is probably because of understory vegetation growth. The ratio of P/TPs is very similar to that of Plot 2 in 2007, and the tree density clearly decreased between 2009 and 2010. The appearance of understory vegetation is already detected in younger trees.

VII. Concluding Remarks

We applied a general four-component scattering decomposition with unitary transformation to ALOS PALSAR polarimetric data collected from 2007 to 2010. The aim was to monitor the yearly variability of planted acacia trees in Indonesia.

The multiyear data analysis revealed the following correlations between the forest structural metrics and decomposition powers: the relative surface scattering power decreased significantly, whereas the relative canopy, double-bounce, and helix scattering powers increased with growth. Overall, the relative surface scattering was reduced as the bare ground became covered with forest growth. On the other hand, the vegetation cover increased the relative canopy and helix scatterings. Decreased correlation of the double-bounce scattering was led by both lower relative double-bounce scattering power in the healthy mature forest and higher scattering power in the damaged forests.

Furthermore, our results suggest that the forest structural conditions can be understood from the yearly variations of the polarimetric parameters, in ways that cannot be elucidated by general correlation analysis. The forest scattering mechanisms could be comprehensively understood by supplementing the results of yearly variations in the polarimetric parameters with forest inventory data obtained by forest measurement and visual assessment of stand conditions. The main findings and their supporting explanations are summarized below.

1) After the rapid growth phase, when the trees retain fewer leaves, canopy scattering is contributed by both forest canopy and understory vegetation. Four-component power decomposition is useful for distinguishing the growth of the canopy itself from growth of the understory vegetation. Increase in the relative canopy scattering accompanied by decrease in the relative helix scattering indicates the growth of understory vegetation. Meanwhile, increase in both canopy and helix scatterings indicates canopy growth/expansion.
2) In the investigated plantation, the relative canopy scattering increases in healthy mature stands before harvest time, because the remaining tree canopy is supplemented by understory vegetation. At the same time, the understory growth strongly interferes with the double-bounce scattering, in which remarkable decrease is observed. This result indicates that the understory conditions must be considered in the analysis of L-band SAR data, especially in this plantation and other sparse forests.
3) Physical leaf damage is associated with a distinct decrease in relative canopy scattering, and also by increased relative surface and double-bounce scatterings. This partial damage in a forest compartment is reflected in the ALOS PALSAR data. Moreover, the fluctuation in the canopy scattering reflects the growing conditions and provides useful information for measuring growth states, even in younger forest stands.

Utilization of polarimetric L-band SAR data in forest management and monitoring is strongly suggested. This study on a single-layered forest elucidated several detailed scattering characteristics. Such understanding will assist forestry researchers to interpret scattering mechanisms in natural forests. Besides, the second generation of ALOS was launched on May 24, 2014. ALOS-2/PALSAR-2 is now in orbit equipped with fully polarimetric and high-resolution imaging mode. The results of this study could be useful for interpretation of the ALOS2 data. In future studies, the backscattering mechanism from plantations should be further clarified by comparing other various polarimetric parameters and by investigating data of a statistically significant sample size. A complete understanding of these mechanisms will lead to novel methods for biomass estimation. At the same time, identification of timber plantations from natural forest area by means of polarimetric information is an important issue, which is left as a future study.

ACKNOWLEDGMENT

The authors are deeply grateful to the staff of the R&D and Planning Sections of the MHP Company for their kind and continuous support during our field surveys.

REFERENCES

[1] Food and Agriculture Organization of United Nations (FAO), "Global planted forests thematic study: results and analysis," in *Planted Forests and Trees Working Paper 38*, A. del Lungo, J. Bal, and J. Carle, Eds. Rome, Italy: Food and Agriculture Organization of United Nations, 2006.
[2] M. Whittle, S. Quegan, Y. Uryu, M. Stüewe, and K. Yulianto, "Detection of tropical deforestation using ALOS-PALSAR: A Sumatran case study," *Remote Sens. Environ.*, vol. 124, pp. 83–98, 2012.
[3] M. Tanase, J. de la Riva, M. Santoro, F. Pérez-Cabello, and E. Kasischke, "Sensitivity of SAR data to post-fire forest regrowth in Mediterranean and boreal forests," *Remote Sens. Environ.*, vol. 115, pp. 2075–2085, 2011.
[4] J. Reiche, C. Souzax, D. H. Hoekman, J. Verbesselt, H. Persaud, and M. Herold, "Feature level fusion of multi-temporal ALOS PALSAR and Landsat data for mapping and monitoring of tropical deforestation and forest degradation," *IEEE J. Sel. Topics Appl. Earth Observ. Remote Sens.*, vol. 6, no. 5, pp. 2159–2173, Oct. 2013.
[5] T. Shiraishi, T. Motohka, R. B. Thapa, M. Watanabe, and M. Shimada, "Comparative assessment of supervised classifiers for land use–Land cover classification in a tropical region using time-series PALSAR mosaic data," *IEEE J. Sel. Topics Appl. Earth Observ. Remote Sens.*, vol. 7, no. 4, pp. 1186–1199, Apr. 2014.
[6] E. T. A. Mitchard *et al.*, "Measuring biomass changes due to woody encroachment and deforestation/degradation in a forest–Savanna boundary region of central Africa using multi-temporal L-band radar backscatter," *Remote Sens. Environ.*, vol. 115, pp. 2861–2873, 2011.
[7] O. Cartus, M. Santoro, and J. Kellndorfer, "Mapping forest aboveground biomass in the Northeastern United States with ALOS PALSAR dual-polarization L-band," *Remote Sens. Environ.*, vol. 124, pp. 466–478, 2012.
[8] J. M. B. Carreiras, M. J. Vasconcelos, and R. M. Lucas, "Understanding the relationship between aboveground biomass and ALOS PALSAR data in the forests of Guinea-Bissau (West Africa)," *Remote Sens. Environ.*, vol. 121, pp. 426–442, 2012.
[9] G. Sandberg, L. M. H. Ulander, J. E. S. Fransson, J. Holmgren, and T. Le Toan, "L- and P-band backscatter intensity for biomass retrieval in hemiboreal forest," *Remote Sens. Environ.*, vol. 115, pp. 2874–2886, 2011.
[10] S. Englhart, V. Keuck, and F. Siegert, "Aboveground biomass retrieval in tropical forests—The potential of combined X- and L-band SAR data use," *Remote Sens. Environ.*, vol. 115, pp. 1260–1271, 2011.
[11] M. Santoro *et al.*, "Retrieval of growing stock volume in boreal forest using hyper-temporal series of Envisat ASAR ScanSAR backscatter measurements," *Remote Sens. Environ.*, vol. 115, pp. 490–507, 2011.
[12] O. Antropov, Y. Rauste, H. Ahola, and T. Hame, "Stand-level stem volume of boreal forests from spaceborne SAR imagery at L-Band," *IEEE J. Sel. Topics Appl. Earth Observ. Remote Sens.*, vol. 6, no. 1, pp. 35–44, Feb. 2013.
[13] J. A. Richards, *Remote Sensing With Imaging Radar*. New York, NY, USA: Springer, 2009.
[14] A. Freeman and S. L. Durden, "A three-component scattering model for polarimetric SAR data," *IEEE Trans. Geosci. Remote Sens.*, vol. 36, no. 3, pp. 963–973, May 1998.
[15] S. R. Cloude and E. Pottier, "An entropy based classification scheme for land applications of polarimetric SAR," *IEEE Trans. Geosci. Remote Sens.*, vol. 35, no. 1, pp. 68–78, Jan. 1997.
[16] Y. Yamaguchi, T. Moriyama, M. Ishido, and H. Yamada, "Four-component scattering model for polarimetric SAR image decomposition," *IEEE Trans. Geosci. Remote Sens.*, vol. 43, no. 8, pp. 1699–1706, Aug. 2005.

[17] Y. Yamaguchi, A. Sato, W. M. Boerner, R. Sato, and H. Yamada, "Four-component scattering power decomposition with rotation of coherency matrix," *IEEE Trans. Geosci. Remote Sens.*, vol. 49, no. 6, pp. 2251–2258, Jun. 2011.
[18] G. Singh, Y. Yamaguchi, and S. E. Park, "General four-component scattering power decomposition with unitary transformation of coherency matrix," *IEEE Trans. Geosci. Remote Sens.*, vol. 51, no. 5, pp. 3014–3022, May 2013.
[19] F. Garestier, P. C. Dubois-Fernandez, D. Guyon, and T. Le Toan, "Forest biophysical parameter estimation using L-and P-band polarimetric SAR data," *IEEE Trans. Geosci. Remote Sens.*, vol. 47, no. 10, pp. 3379–3388, Oct. 2009.
[20] F. Goncalves, J. Santos, and R. Treuhaft, "Stem volume of tropical forests from polarimetric radar," *Int. J. Remote Sens.*, vol. 32, pp. 503–522, 2011.
[21] J. M. Austin, B. G. Mackey, and K. P. Van Niel, "Estimating forest biomass using satellite radar: An exploratory study in a temperate Australian Eucalyptus forest," *For. Ecol. Manage.*, vol. 176, pp. 575–583, 2003.
[22] F. F. Gama, J. R. Dos Santos, and J. C. Mura, "Eucalyptus biomass and volume estimation using interferometric and polarimetric SAR data," *Remote Sens.*, vol. 2, pp. 939–956, 2010.
[23] F. M. Henderson, R. A. Ryerson, and A. J. Lewis, and American Society for Photogrammetry and Remote Sensing, *Principles and Applications of Imaging Radar*. Hoboken, NJ, USA: Wiley, 1998.
[24] M. Santoro, J. E. S. Fransson, L. E. B. Eriksson, M. Magnusson, L. M. H. Ulander, and H. Olsson, "Signatures of ALOS PALSAR L-band backscatter in Swedish forest," *IEEE Trans. Geosci. Remote Sens.*, vol. 47, no. 12, pp. 4001–4019, Dec. 2009.
[25] H. Balzter, J. R. Baker, M. Hallikainen, and E. Tomppo, "Retrieval of timber volume and snow water equivalent over a Finnish boreal forest from airborne polarimetric Synthetic Aperture Radar," *Int. J. Remote Sens.*, vol. 23, pp. 3185–3208, 2002.
[26] C. S. Rowland, H. Balzter, T. P. Dawson, A. Luckman, G. Patenaude, and L. Skinner, "Airborne SAR monitoring of tree growth in a coniferous plantation," *Int. J. Remote Sens.*, vol. 29, pp. 3873–3889, 2008.
[27] G. Macelloni, S. Paloscia, P. Pampaloni, F. Marliani, and M. Gai, "The relationship between the backscattering coefficient and the biomass of narrow and broad leaf crops," *IEEE Trans. Geosci. Remote Sens.*, vol. 39, no. 4, pp. 873–884, Apr. 2001.
[28] S. Kobayashi, R. Widyorini, S. Kawai, Y. Omura, K. Sanga-Ngoie, and B. Supriadi, "Backscattering characteristics of L-band polarimetric and optical satellite imagery over planted acacia forests in Sumatra, Indonesia," *J. Appl. Remote Sens.*, vol. 6, p. 063525, 2012.
[29] S. Kobayashi *et al.*, "Characteristics of decomposition powers of L-band multi-polarimetric SAR in assessing tree growth of industrial plantation forests in the tropics," *Remote Sens.*, vol. 4, pp. 3058–3077, 2012.
[30] S. Kawai and R. Widyorini, "Sustainable forest management and regional environment in South-East Asia," in *Proc. 2nd Int. Conf. Kyoto Univ. Global COE Program Search Sustain. Humanosphere Asia Africa*, Kyoto, Japan, 2008, pp. 1–4.
[31] R. Gunawan and R. Wahyono, "Faktor bentuk (form factor) Acacia mangium (in Indonesian)," Research and Development Division, PT. Musi Hutan Persada, 2004, vol. 14, no. 1.
[32] Y. Yamaguchi, *Radar Polarimetry from Basic to Applications: Radar Remote Sensing using Polarimetric Information (in Japanese)*. Tokyo, Japan: Institute of Electronics, Information, and Communication Engineers, 2007.
[33] Q. S. He *et al.*, "Forest stand biomass estimation using ALOS PALSAR data based on LiDAR-derived prior knowledge in the Qilian Mountain, western China," *Int. J. Remote Sens.*, vol. 33, pp. 710–729, 2012.
[34] R. A. Ryerson, F. M. Henderson, and A. J. Lewis, and American Society for Photogrammetry and Remote Sensing, *Manual of Remote Sensing, Principles and Applications of Imaging Radar*. Hoboken, NJ, USA: Wiley, 1998.
[35] M. S. Fujita, D. M. Prawiradilaga, and T. Yoshimura, "Roles of fragmented and logged forests for bird communities in industrial Acacia mangium plantations in Indonesia," *Ecol. Res.*, vol. 29, pp. 741–755, 2014.
[36] H. G. Jones and R. A. Vaughan, *Remote Sensing of Vegetation: Principles, Techniques, and Applications*. London, U.K.: Oxford Univ. Press, 2010.

Shoko Kobayashi, photograph and biography not available at the time of publication.

Yoshiharu Omura, photograph and biography not available at the time of publication.

Kazadi Sanga-Ngoie, photograph and biography not available at the time of publication.

Yoshio Yamaguchi, photograph and biography not available at the time of publication.

Ragil Widyorini, photograph and biography not available at the time of publication.

Motoko S. Fujita, photograph and biography not available at the time of publication.

Bambang Supriadi, photograph and biography not available at the time of publication.

Shuichi Kawai, photograph and biography not available at the time of publication.